Testing lunar permanently shadowed regions for water ice: LEND results from LRO

A. B. Sanin,[1] I. G. Mitrofanov,[1] M. L. Litvak,[1] A. Malakhov,[1] W. V. Boynton,[2] G. Chin,[3] G. Droege,[2] L. G. Evans,[4] J. Garvin,[3] D. V. Golovin,[1] K. Harshman,[2] T. P. McClanahan,[3] M. I. Mokrousov,[1] E. Mazarico,[3] G. Milikh,[5] G. Neumann,[3] R. Sagdeev,[5] D. E. Smith,[6] R. D. Starr,[7] and M. T. Zuber[6]

Received 22 September 2011; revised 19 April 2012; accepted 30 April 2012; published 15 June 2012.

[1] We use measurements from the Lunar Exploration Neutron Detector (LEND) collimated sensors during more than one year of the mapping phase of NASA's Lunar Reconnaissance Orbiter (LRO) mission to make estimates of the epithermal neutron flux within known large Permanently Shadowed Regions (PSRs). These are compared with the local neutron background measured outside PSRs in sunlit regions. Individual and collective analyses of PSR properties have been performed. Only three large PSRs, Shoemaker and Cabeus in the south and Rozhdestvensky U in the north, have been found to manifest significant neutron suppression. All other PSRs have much smaller suppression, only a few percent, if at all. Some even display an excess of neutron emission in comparison to the sunlit vicinity around them. Testing PSRs collectively, we have not found any average suppression for them. Only the group of 18 large PSRs, with area >200 km^2, show a marginal effect of small average suppression, ∼2%, with low statistical confidence. A ∼2% suppression corresponds to ∼125 ppm of hydrogen taking into account the global neutron suppression near the lunar poles and assuming a homogeneous H distribution in depth in the regolith. This means that all PSRs, except those in Shoemaker, Cabeus and Rozhdestvensky U craters, do not contain any significant amount of hydrogen in comparison with sunlit areas around them at the same latitude.

Citation: Sanin, A. B., et al. (2012), Testing lunar permanently shadowed regions for water ice: LEND results from LRO, *J. Geophys. Res.*, *117*, E00H26, doi:10.1029/2011JE003971.

1. Introduction

[2] More than 50 years ago, it was suggested that some areas near the lunar poles are sufficiently cold to trap and preserve for a very long time (∼Gy) hydrogen bearing volatiles, either primordial or produced at the Moon via solar wind interactions or brought to the Moon as water ice by comets and meteoroids [*Watson et al.*, 1961; *Arnold*, 1979]. In the 1990s, observations made by the bistatic radar instrument onboard the Clementine spacecraft identified some anomalous regions on the Moon associated with permanently shadowed regions (PSRs) that were consistent with the presence of water ice [*Nozette et al.*, 1996, 2001; *Simpson and Tyler*, 1999]. These observations have been criticized as ambiguous [*Fa et al.*, 2011]. Another attempt to test lunar PSRs for water was performed using neutron (LPNS) and gamma-ray (LPGRS) spectrometers onboard the Lunar Prospector mission launched in 1998 [*Feldman et al.*, 2004]. These instruments were able to create global elemental and neutron albedo maps and discover significant reductions of epithermal neutron fluxes in lunar polar regions poleward of 70°S and 70°N latitudes. This result was interpreted as an enhancement of hydrogen abundance in these areas [*Feldman et al.*, 2001; *Lawrence et al.*, 2006].

[3] The advantage of nuclear methods over other remote sensing techniques is that they offer greater sensitivity to hydrogen (down to 100 ppm) plus the ability to probe to depths down to 1 m. Regional variations of neutron flux were observed by LPNS using its omni-directional sensors with poor spatial resolution relative to the smaller scales of most PSRs [*Maurice et al.*, 2004].

[4] It has been shown that neutrons emitted from a planetary body with different energies are sensitive to soil composition.

[1]Institute for Space Research, RAS, Moscow, Russia.
[2]Lunar and Planetary Laboratory, University of Arizona, Tucson, Arizona, USA.
[3]NASA Goddard Space Flight Center, Greenbelt, Maryland, USA.
[4]Computer Sciences Corporation, Lanham, Maryland, USA.
[5]Space Physics Department, University Maryland, College Park, Maryland, USA.
[6]Department of Earth, Atmospheric and Planetary Sciences, MIT, Cambridge, Massachusetts, USA.
[7]Catholic University of America, Washington, D. C., USA.

Corresponding author: A. B. Sanin, Institute for Space Research, RAS, Moscow, 117997, Russia. (sanin@mx.iki.rssi.ru)

The thermal neutron flux is dependent on the abundance of elements such as Fe, Ti, Gd, Sm. The fast neutron flux is proportional to the average atomic mass of the regolith and can serve as a marker that distinguishes between surface materials enriched with heavier elements (e.g., iron in the nearside of the mare basins) and lighter elements (aluminum in the far side highlands). These effects were clearly visible in global maps provided by LPNS [*Feldman et al.*, 1998a, 1998b; *Elphic et al.*, 1998; *Gasnault et al.*, 2001] and the recently processed LEND maps discussed by *Litvak et al.* [2012].

[5] But the most intriguing result concerns deconvolution of regional variations of epithermal neutrons around lunar poles at a scale comparable with the size of large craters. It is thought that the distribution of epithermal neutrons in these regions is controlled by the hydrogen abundance. More than 10 years ago, LPNS found that the average neutron suppression in the epithermal energy range increases poleward from 70°, both in the South and the North, by 4–5% [*Feldman et al.*, 1998b, 2001]. But the spatial resolution of these measurements was greater than most PSRs (FWHM = 44 km [*Maurice et al.*, 2004; *Lawrence et al.*, 2006]), requiring model dependent data deconvolution of smaller surface features and the inference that hydrogen may concentrate at the bottom of permanently shadow craters [*Eke et al.*, 2009, *Elphic et al.*, 2007].

[6] From these results, the ensuing decade witnessed an ongoing series of sophisticated scientific investigations, discussions, and speculations regarding the interpretation of these phenomena: was hydrogen localized in cold traps within PSRs and could hydrogen abundances be so high that it indicated the presence of water ice? Some publications indicated PSRs may contain up to 1.5% of water equivalent hydrogen presumably in the form of water ice from comets, while other research postulated that at least half of this content could be hydrogen bearing volatiles created by solar wind interactions with the regolith, which subsequently migrated to the cold poles through micrometeoritic bombardment processes [*Crider and Vondrak*, 2000, 2003].

[7] Recent experimental observations from the Indian Space Research Organization (ISRO) Chandrayaan-1 mission, the NASA Lunar Reconnaissance Orbiter (LRO) and the Lunar Crater Observation and Sensing Satellite (LCROSS) missions add significantly to the discussion. The recent orbital radar observations of the Lunar North pole (MiniSAR onboard Chandrayaan-1) indicate differences in circular polarization ratios comparing the interior and exterior of some polar shadowed craters, which suggest the presence of water ice [*Spudis et al.*, 2010]. Near-infrared spectral data have shown surficial hydrogen as either H_2O or OH is spread widely across the lunar poles, at depths up to ~1 mm (which is the approximate sampling depth of the near-IR instruments), and could have an abundance of ~100–1000 ppm H_2O [*Pieters et al.*, 2009; *Sunshine et al.*, 2009; *Clark*, 2009]. The LCROSS spacecraft observed the impact of its launch vehicle upper stage within the PSR of the south polar crater Cabeus and observed 5.6 ± 2.9% of water by mass in the plume [*Colaprete et al.*, 2010].

[8] The most recent attempt using nuclear methods was made by the Lunar Exploration Neutron Detector (LEND) instrument onboard LRO [*Mitrofanov et al.*, 2008, 2010a]. LEND is multiband neutron spectrometer system similar to LPNS but equipped with a neutron collimator that significantly reduces incoming epithermal and thermal neutrons to the detector from non-nadir angles and yields an instrument footprint ~10 km in diameter (Full Width at Half Maximum, FWHM, assuming the altitude of the spacecraft is about 50 km). Furthermore, LEND's field of view (FOV) is comparable with the size of many large PSRs of interest and provides additional capability to contrast neutron fluxes from the interior and exterior of shadowed regions. Preliminary analysis of LEND measurements was performed during the evaluation of potential impact targets for the LCROSS mission to quantify water content in the regolith. From these results it was shown that the physics of enhanced hydrogen regions was more complicated than was initially expected [*Mitrofanov et al.*, 2010b]. Some PSRs, like Cabeus and Shoemaker, are quite distinguishable with clear suppression of epithermal neutrons inside the crater compared with the fluxes in neighboring regions. These regional suppressions were interpreted as an indication of high hydrogen abundance and possibly water-ice deposits. But many other PSRs indicated no difference between the neutron fluxes in the PSR and neighboring sunlit areas.

[9] In this paper, we present the first systematic analysis of neutron emission from PSRs. LEND data gathered during the primary part of the LRO mapping phase, which started on September 15, 2009, are used for this analysis and we have implemented several methods to compare fluxes in shadowed and sunlit regions at the same latitudes. A primary objective of this paper is to determine if all individual PSRs or a group of PSRs with small, medium or large areas contain a significant amount of water ice in the upper ~1 m of regolith in comparison with hydrogen content in the regolith of sunlit areas at the same latitude. The general smooth poleward increase of hydrogen content in the regolith observed by all neutron experiments at the Moon is not a subject of this paper.

2. Instrumentation, Data Reduction and Methods

2.1. Instrumentation

[10] LEND is a neutron spectrometer with the ability to globally map neutron fluxes in different energy ranges including thermal, epithermal and fast neutrons. LEND also has the capability to measure epithermal neutrons with spatial resolution of about 10 km at the poles (see *Mitrofanov et al.* [2008, 2010a] for details).

[11] The LEND mapping of regional variations of epithermal neutron flux across the lunar surface is supported using both an uncollimated detector Sensor for Epithermal Neutrons (SETN) with spatial resolution similar to LPNS (see global maps from this detector presented by *Litvak et al.* [2012] and the four Collimated Sensors for Epithermal Neutrons (CSETN1–4). The CSETN1–4 provide high spatial resolution observations, FWHM ~10 km [*Mitrofanov et al.*, 2008, 2010a]. The mapping of the SETN detector is similar to the measurement techniques applied to the LPNS instrument. The CSETN1–4 ^{3}He gas proportional counters are surrounded by a collimator that defines the aperture. The collimator sides and bottom are covered with cadmium and ^{10}B [*Mitrofanov et al.*, 2008, 2010a].

[12] Measurements made by the LEND collimated sensors are the primary object of this work, providing the unique possibility of measuring regions inside large craters with surface areas more than ~100 km^2 and to evaluate the local suppression or excess of epithermal neutron fluxes.

2.2. Data Reduction

[13] In our analysis, we used LEND maps created from Planetary Data System (PDS) data including the period from September 15, 2009 up to December 15, 2010. A number of calibration processing procedures were applied to the raw LEND counting rates prior to mapping (see M. L. Litvak et al., LEND neutron data processing for the mapping of the Moon, submitted to *Journal of Geophysical Research*, 2012; and W. Boynton et al., High spatial resolution of epithermal neutron emission from the lunar poles: Constraints on hydrogen mobility, submitted to *Journal of Geophysical Research*, 2012). This included: correction of counting rates for efficiency saturation effects, adjusting for long-term variation of Galactic Cosmic Rays (GCR), eliminating times of strong Solar Particle Events, separation of charged particle and neutron events, as well as temperature and altitude corrections.

[14] Counting rates during orbital measurement in all LEND detectors are measured with time accumulation intervals of 1 s. For such short time intervals, the spacecraft flies over a surface distance of about ~1.6 km. This is short enough to distinguish local landforms with sizes 10×10 km. For our analysis we have created polar map grids with a pixel size 1/2 degree longitude by 1/16 degree latitude. The latitudinal pixel size is comparable to the 1.6 km distance. All counts measured by LEND collimated detectors were directly distributed into the corresponding pixels of this map grid with counting rate, exposure time and statistical error in each pixel.

2.3. Testing Analysis of Permanently Shadowed Regions

[15] Several analytical techniques are applied to the LEND high resolution neutron data in this study. The first is to create a detailed map of the distribution of epithermal neutron fluxes across polar regions and to search for local areas indicating significant Neutron Suppression Regions (NSRs) relative to background flux rates. (This analytical technique is described in Boynton et al. (submitted manuscript, 2012) and I. G. Mitrofanov et al. (Testing polar spots of water-rich permafrost on the Moon: LEND observations onboard LRO, submitted to *Journal of Geophysical Research*, 2012).) Localized NSRs can be compared with other available data describing properties of relief (such as elevation, roughness, and slopes directions), solar illumination and temperature distribution (day, night, average temperatures, model predictions of possible ice depth). Another technique is to use known targets and landforms of the lunar surface and to correlate them with variations of epithermal neutron flux. For example, it is suggested that there may be a correlation between the orientation of crater slopes and LEND counting rates [see *McClanahan et al.*, 2012].

[16] In this paper we use the second technique and make estimates of the counting rates within known large PSRs (with area greater than or equal to the LEND footprint) and compare counting rates from the local neutron background measured outside PSR areas (sunlit regions). If our analysis shows that epithermal counting rates measured for PSRs are lower than local background, it would support the hypothesis that PSRs are major hydrogen rich areas on the lunar surface. Depending on the magnitude of this suppression, PSRs may even be considered as a primary target in the search for possible water ice reservoirs.

[17] The LRO instrument payload includes the Lunar Orbiter Laser Altimeter (LOLA), which is specially designed for global mapping of lunar landscape and the creation of a new high resolution topographic map of the Moon [*Smith et al.*, 2010]. After several months of operations the LOLA team was able to produce illumination maps of the lunar poles. The Moon's spin axis is nearly perpendicular to the ecliptic plane, just ~1.5° away from the ecliptic pole. This creates natural conditions where sunlight never directly reaches the floor of some of the deepest craters in both North and South circumpolar regions. The new illumination maps provided by LOLA represent the percentage of time that the Sun was visible from a given point on the surface [*Mazarico et al.*, 2011]. If the average solar illumination during the lunar precession period is equal to zero for some surface element, then it is defined as a part of a PSR. Clusters of contiguous pixels may be aggregated to define a single PSR. The full list of all PSRs both at the North and South poles consists of more than several thousand areas ranging from very small (<1 km^2) up to quite large regions of more than 1000 km^2. For the South pole, the total number of PSRs is smaller than for the North, but on average the southern PSRs are larger with several tens of PSRs having areas more than 100 km^2. The set selected for analysis in this study all have areas >100 km^2. The list of tested PSRs is presented in Table 1.

2.4. Local Background

[18] To perform our analysis of PSRs we need to derive two key observational parameters: 1) the counting statistics across each PSR's pixels and 2) the counting statistics acquired across neighboring sunlit areas, which we define as a local background. The latter value is based on some a priori information, and can be estimated by various methods. We assume the best option is to consider nearby sunlit areas having the same soil type and a large enough surface to get significantly large number of accumulated counts, much larger than ones derived from the PSR area. This selection criterion is necessary to ensure that possible variations between these two parameters are due to different H abundances and not due to regolith elemental variations. Our goal is to compare neutron flux inside PSRs with fluxes in surrounding sunlit areas to find local effect between shadowed and sunlit areas at the same latitude. The last condition is important because in earlier observations LPNS revealed the existence of extended neutron suppression which depends on the latitude. This extended neutron suppression shows a decrease in epithermal neutron flux as a function of increasing latitude poleward of 70° South and North. Therefore, the area selected for the estimation of local background should be located at the same latitude belt as the tested PSR.

[19] Our first simple, conservative option for an estimation of local background around test PSRs is based on latitude analysis. We have averaged the LEND polar maps (see Figure 1) by longitude and created latitude band profiles of counting rates. All permanently shadow pixels have been excluded from averaging. The resulting profile shows a latitude dependence of counting rate for polar regions for sunlit areas only (see Figures 2 and 3). For each analyzed PSR we estimate the value of the local background using this profile, as the counting rate at the latitude belt containing the PSR itself. This option takes into account the latitude dependence of the neutron flux distribution across polar

Table 1. Properties of PSRs With Areas >100 km^2

Name of Crater-Contained PSR or Nearest Crater	PSR Area (km^2)	Exposure (sec)	Min Lon (deg)	Max Lon (deg)	Min Lat (deg)	Max Lat (deg)	Local Suppression 1	Local Suppression 2
Shoemaker[a]	**1079.99**	**20065.88**	**27.0**	**63.5**	**−88.6**	**−87.4**	**−5.5% ±1.2%**	**−6.3% ± 1.1%**
Haworth	1019.21	12883.67	−17.3	12.5	−88.1	−86.9	−1.4% ± 1.5%	−2.1% ± 1.4%
Faustini	665.25	4315.42	74.1	94.2	−87.6	−86.7	−2.0% ± 2.6%	−2.1% ± 2.6%
Sverdrup	550.53	11832.28	−161.0	−123.0	−88.6	−87.8	−1.3% ± 1.6%	−1.7% ± 1.6%
Amundsen	405.20	686.13	87.0	95.3	−83.8	−83.0	9.3% ± 6.6%	10.2% ± 6.6%
Rozhdestvenskiy U	**390.68**	**1676.84**	**148.3**	**158.1**	**84.2**	**85.0**	**−11.3% ± 3.9%**	**−10.6% ± 3.9%**
Cabeus B	382.29	976.05	−57.4	−51.9	−82.0	−81.3	4.4% ± 5.3%	5.2% ± 5.3%
Lovelace	339.32	906.26	−112.7	−107.4	81.1	81.8	2.5% ± 5.7%	3.1% ± 5.6%
Idel'son L	325.90	1103.30	115.2	121.9	−84.2	−83.5	−7.7% ± 4.9%	−7.4% ± 4.8%
Sylvester	320.69	545.91	−84.4	−78.6	81.7	82.2	2.4% ± 7.1%	3.6% ± 7.1%
Malapert C (PSR is out of the crater)	306.92	851.43	8.5	13.4	−82.5	−81.7	2.8% ± 5.7%	2.7% ± 5.7%
Cabeus	**283.09**	**1188.81**	**−50.4**	**−42.6**	**−84.7**	**−84.1**	**−14.4% ± 4.7%**	**−14.9% ± 4.7%**
Lenard	281.42	940.32	−113.1	−104.4	84.4	85.1	−3.0% ± 5.5%	−3.6% ± 5.5%
de Gerlache	242.47	1940.03	−101.4	−78.0	−88.6	−88.0	−2.0% ± 3.7%	−2.5% ± 3.7%
Rozhdestvenskiy K	241.18	545.07	−148.2	−143.5	81.3	82.1	−6.1% ± 6.9%	−4.8% ± 6.9%
Nansen F	225.26	893.82	59.0	66.3	83.9	84.6	3.8% ± 5.8%	4.0% ± 5.7%
Haworth (PSR at flat terrain out of the crater)	222.92	1245.08	16.3	26.8	−87.1	−86.3	−6.3% ± 4.6%	−6.7% ± 4.6%
Hermite A	211.49	3118.60	−60.6	−44.5	87.7	88.2	−1.7% ± 2.9%	−2.3% ± 2.8%
Wiechert	193.29	663.39	160.6	166.2	−84.0	−83.4	1.3% ± 6.4%	1.4% ± 6.4%
Malapert	190.86	742.75	3.0	8.5	−84.4	−83.8	0.3% ± 6.0%	0.9% ± 6.0%
Faustini (PSR out of the crater)	182.81	1143.60	106.2	127.4	−88.3	−87.8	−3.8% ± 4.8%	−3.9% ± 4.8%
Nobile	177.55	703.43	57.5	63.5	−84.8	−84.2	−9.8% ± 6.2%	−10.4% ± 6.2%
Scott E	167.54	389.92	34.0	37.4	−81.1	−80.7	5.2% ± 8.4%	5.6% ± 8.3%
Nefed'ev	148.62	190.85	133.3	137.6	−80.5	−80.1	−21.1% ± 11.3%	−21.0% ± 11.3%
Cabeus (PSR is out of the crater)	142.89	507.51	−23.3	−19.3	−84.0	−83.5	−7.0% ± 7.2%	−6.9% ± 7.2%
Sylvester N	141.68	306.36	−70.3	−67.0	82.1	82.5	−3.8% ± 9.1%	−3.4% ± 9.1%
Lovelace E	138.35	218.93	−98.3	−95.3	81.7	82.2	10.1% ± 12.1%	11.5% ± 12.1%
Nobile	136.06	544.73	46.7	53.5	−85.6	−85.1	0.4% ± 7.0%	−0.4% ± 7.0%
Nansen A	134.39	323.14	62.7	65.9	81.9	82.4	3.9% ± 9.7%	5.2% ± 9.7%
Nobile	129.60	699.84	45.4	53.0	−86.6	−86.1	−10.7% ± 6.2%	−11.0% ± 6.1%
Amundsen (PSR is in a nearby large crater)	126.02	351.44	64.9	69.8	−83.2	−82.8	−3.6% ± 8.9%	−2.4% ± 8.9%
Amundsen	125.13	160.97	79.9	84.7	−83.5	−83.0	−2.3% ± 14.0%	−1.1% ± 14.0%
Cabeus	123.33	542.28	−54.9	−49.3	−85.6	−85.2	−7.0% ± 7.0%	−7.7% ± 7.0%
Malapert (PSR is in a nearby crater)	123.20	301.83	−6.6	−3.1	−82.6	−82.2	11.4% ± 9.7%	11.8% ± 9.7%
Haworth (PSR at flat terrain out of the crater)	120.32	876.85	27.9	35.1	−86.6	−86.2	6.3% ± 5.6%	5.5% ± 5.5%
Fibiger	118.60	848.99	33.7	40.5	85.8	86.2	−4.4% ± 5.7%	−5.3% ± 5.7%
Houssay	116.15	163.10	97.2	100.2	82.7	83.2	0.8% ± 12.9%	2.7% ± 12.9%
Wiechert U	114.44	183.13	147.4	151.6	−83.5	−83.0	−11.6% ± 11.5%	−10.7% ± 11.5%
Rozhdestvenskiy (PSR is on the crater's wall)	113.99	228.57	−163.8	−161.0	82.1	82.6	−15.6% ± 10.5%	−14.5% ± 10.5%
Malapert (PSR is in a nearby crater)	112.96	298.29	6.8	9.7	−83.1	−82.5	17.1% ± 9.8%	18.0% ± 9.8%
Wiechert E	111.21	347.33	174.0	177.7	−83.6	−83.2	2.2% ± 8.8%	3.0% ± 8.7%
Plaskett V	108.63	160.12	119.2	122.6	81.4	81.7	13.3% ± 13.3%	14.2% ± 13.3%
Plaskett S	103.91	209.56	149.2	151.6	80.7	81.1	−12.4% ± 10.9%	−10.9% ± 10.9%
Nansen E (PSR is out of the crater)	102.87	104.76	80.0	84.6	82.9	83.2	−16.1% ± 16.1%	−13.9% ± 16.0%
Mouchez M	100.78	162.82	−51.2	−49.0	79.9	80.3	0.1% ± 12.7%	0.5% ± 12.7%
Malapert	100.35	384.52	−0.6	3.8	−84.7	−84.4	16.2% ± 8.5%	15.1% ± 8.5%

[a]Bold font indicates there are only three PSRs that have significant neutron suppression relative to local background.

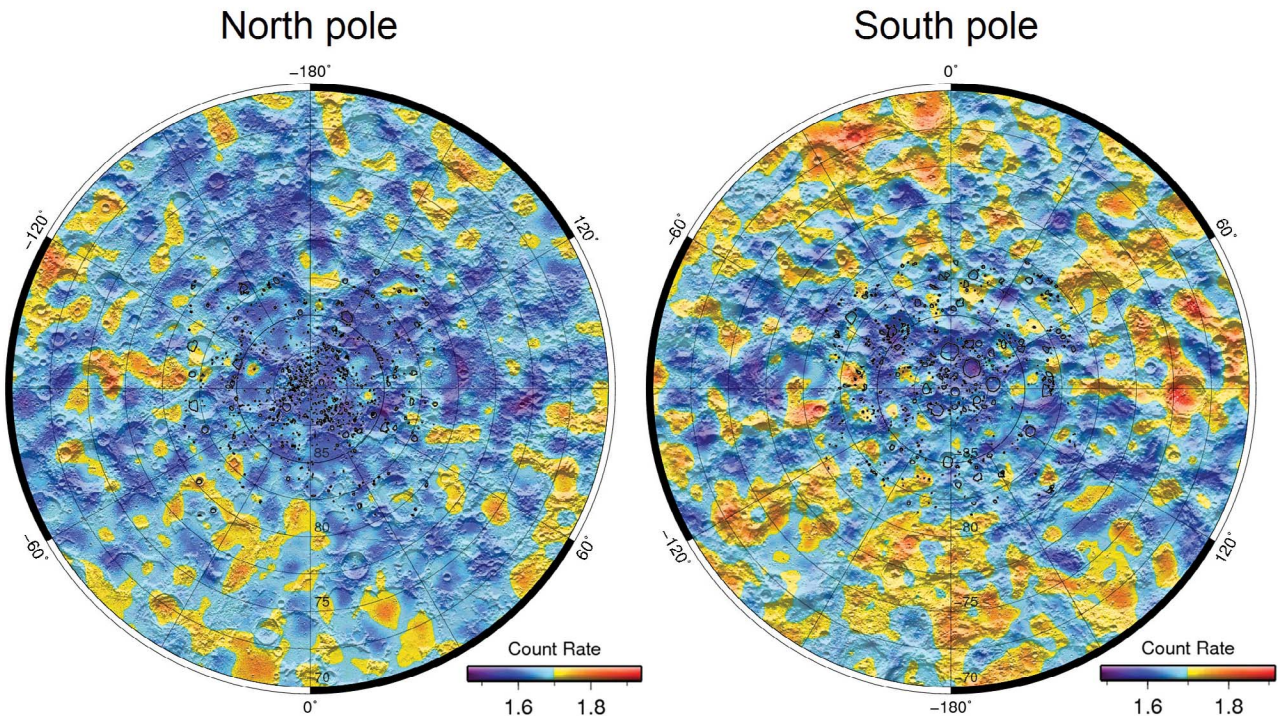

Figure 1. LEND map of epithermal neutrons at the lunar poles. Raw counting rate maps are smoothed to decrease random fluctuations. Smoothing scale increases outward from the poles to produce similar counting statistics at all latitudes. Black spots and contours of the maps represent the boundaries of PSRs according to LOLA data [*Mazarico et al.*, 2011].

regions, significantly increases the counting statistics and decreases the statistical error in the estimation of local background. However, it may not account for a possible longitude asymmetry of neutron flux suppression around the poles.

[20] Another background estimation technique is more complex and uses a two-dimensional approach. In this case we again take the original polar maps of the LEND counting rate, but smooth with a Gaussian filter of pre-selected full width at half maximum (FWHM) much larger than size of PSRs, excluding in the smoothing process all known permanently shadowed pixels. On this map all pixels within PSRs are filled by values predicted by the Gaussian smoothing process based on surrounding sunlit pixels. This approach provides an estimate of the local background counting rates from the sunlit vicinity around the selected PSR location. The disadvantage of this method is that we do

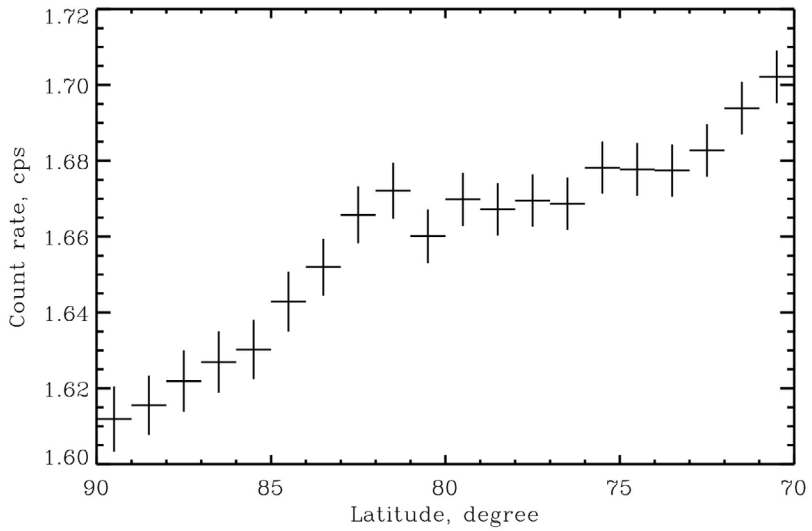

Figure 2. Latitude profile of counting rate averaged over 1° latitudinal belts for North polar region. Statistical uncertainties are shown as vertical error bars.

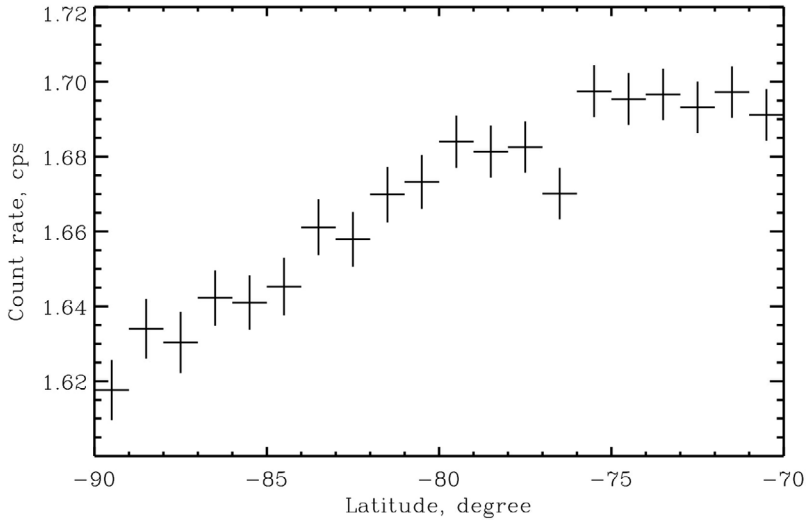

Figure 3. Latitude profile of counting rate averaged over 1° latitudinal belts for South polar region. Statistical uncertainties are shown as vertical error bars.

not know by definition the best FWHM for the smoothing filter. Too small a filter size will provide an estimate of local background with significant uncertainty due to poor statistics. Too large a filter size will smooth out the effect of extended polar suppression of neutron flux. For testing large PSRs, we will use the smoothing filter with the distance scale of ∼227 km = 7.5° of latitude (see below). The selected scale is the distance on the lunar surface from sub-LRO point to the horizon visible from the spacecraft at 50 km altitude orbit (this distance is ∼412 km) multiplied by a factor ∼0.55.

3. Testing of Individual PSRs

[21] In this section we present results for testing epithermal neutron emission for large area PSRs with data from the LEND collimated detectors. We have taken time series data gathered from the four LEND collimated detectors for epithermal neutrons distributed across a map grid (as described in section 2) and estimated the average counting rate for each individual PSR having area larger than or comparable with the LEND spatial resolution. Taking into account that the LEND spatial resolution is a spot on the lunar surface with radius ∼5 km, we selected only large PSRs with areas greater than 100 km^2. There are 46 such PSRs, 29 in the South and 17 in the North polar regions. Their areas range from ∼100 km^2 up to >1000 km^2. Eighteen of them have area >200 km^2. The two largest PSRs have areas ∼1000 km^2 (Shoemaker and Haworth). So, about half of the PSR set is significantly larger than the LEND spatial resolution.

[22] All selected PSRs are presented in Table 1 together with their areas, coordinate box (minimum and maximum longitude/latitude limiting the PSR area) and the neutron flux suppression within PSR borders found using two methods of background estimation (see previous section). The values of suppression are presented as the difference, Δ, between the average counting rate estimated for the PSR and the counting rate measured for the surrounding sunlit areas where we assume ∼100 ppm hydrogen in the regolith [*Lawrence et al.*, 2006]. In each case, we also estimated statistical errors to test statistical significance of measured differences. The local neutron suppression parameter is presented in percent according to the expression:

$$P_{\text{sup}} = \frac{\Delta}{1.7} \times 100\%, \tag{1}$$

where the value of 1.7 is the averaged counting rate in the field of view of LEND collimated detectors outside of extended polar suppression region [see *Litvak et al.*, 2012].

[23] We consider the local suppression in a PSR to be significant if it differs from zero by more than three standard deviations or 3σ (this means that only 0.27% of these cases may be the result of a random fluctuation). For any PSR it is possible to find an upper limit (Γ) for its neutron suppression parameter, P_{sup}. This limit is calculated to be the value of the suppression parameter required to make it significant at the 3σ level. The upper limit for local neutron suppression is estimated from the expression:

$$\Gamma = \frac{3\delta}{1.7} \times 100\%, \tag{2}$$

where $\delta = \sqrt{\Delta_{PSR}^2 + \Delta_{bgd}^2}$ - is a total statistical error corresponding to the difference in counting rates between a PSR with uncertainty Δ_{PSR} and local background with uncertainty Δ_{bgd}; the value of 1.7 is the same as in equation (1).

[24] As indicated in Table 1 by bold font, there are only three PSRs that have significant neutron suppression relative to local background:

[25] 1. PSR in crater *Shoemaker* in South circumpolar area which has a suppression value in the range of −5.5% to −6.3% (depending on how neutron suppression is calculated, see above). These values correspond to 220–245 ppm of hydrogen, provided it is homogeneously distributed in the regolith (method of calculation is described in *Mitrofanov et al.* [2010b].

[26] 2. PSR in crater *Cabeus* in South circumpolar area has suppression in the range−14.4% to −14.9%. These values

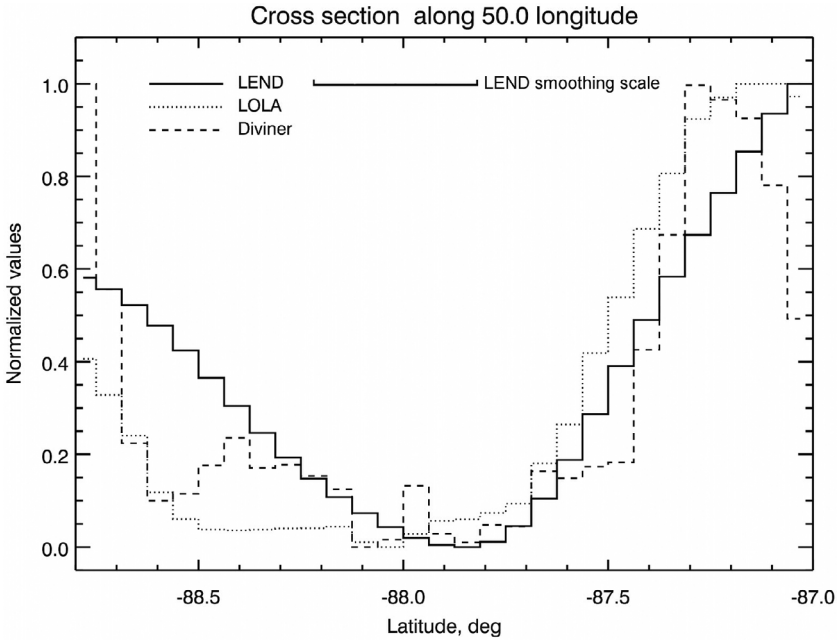

Figure 4. A cross-section in latitude at 50.0° longitude of Shoemaker crater for LEND (solid line), LOLA (dotted line) and Diviner (dashed line) data. The "LEND smoothing scale" corresponds to a FWHM of 10 km in the collimated detectors. Good correlation of minimum values in all three data sets is visible. Maximum hydrogen concentration in this crater is well correlated with crater typography and with minimum of observed average temperature of regolith.

correspond to 460–470 ppm of uniformly distributed hydrogen.

[27] 3. PSR in crater *Rozhdestvensky U* in North circumpolar area which has suppression in the range −10.6% to −11.3%. These values correspond to 345–365 ppm of hydrogen concentration. This is the only PSR in the North circumpolar area with large suppression. Though the significance of suppression in this case is slightly less than 3σ we include it in this set because of its identification with a large crater in the North polar region.

[28] None of the other tested PSRs have a statistically significant suppression of epithermal neutron flux relative to neutron flux from local background. From this result we may conclude that all polar PSRs do not appear to be primarily responsible for the extended suppression of epithermal neutrons observed at the poles, and individual PSRs do not contain large amounts of water ice deposits to a depth of ∼1 m in the regolith.

[29] The epithermal neutron flux suppression of the PSR in Cabeus crater is the largest statistically significant suppression of neutron flux in the South circumpolar area and therefore corresponds to the highest hydrogen abundance in the regolith. As discussed earlier, the PSR in crater Cabeus was the target for the LCROSS impact [see *Colaprete et al.*, 2010]. From this experiment the estimate of water concentration in the soil at the impact site is larger ($5.6 \pm 2.9\%$ by weight) than the value of hydrogen concentration found in this analysis (460–470 ppm). This difference may be explained, in part, by the fact that the LEND result represents an average over the total area of the PSR which is ∼280 km^2 and much large than LCROSS impact site. Also, one may consider a double layer regolith model with a dry top layer a few tens of centimeters thick above an enhanced hydrogen lower layer. In this case, the observed suppression will correspond to increasing hydrogen concentration with increasing thickness of the overlying dry layer [*Mitrofanov et al.*, 2010b].

[30] It is interesting to compare three large southern PSRs in craters Shoemaker (51 km diameter), Haworth (35 km diameter) and Faustini (39 km diameter). These craters have about the same floor depth compared to local terrain, their ages are about the same, and floor average temperatures are similar, less than 60 K for all three (data have been taken from the LOLA and Diviner PDS). But only PSR in Shoemaker manifests statistically significant neutron local suppression with possible concentration of 220–245 ppm of hydrogen in the regolith. To illustrate this result we present in Figure 4 a cross-section in the meridian direction of the crater relief, average surface temperature and measured neutron flux. Only in the case of Shoemaker crater does the maximum of hydrogen concentration correlate with both the crater floor and also with the minimum observed average temperature of the regolith. A slight shift of maximum hydrogen concentration from the crater's center in the equatorial direction is in agreement with results obtained in *McClanahan et al.* [2012]. Upper limits of neutron suppression, Γ, for the PSRs in Haworth and Faustini craters are equal to −4.3% and −7.9%, respectively. This means that in these two PSRs there is no hydrogen concentration larger than 195 ppm and 275 ppm, respectively.

[31] In the case of the PSR in Cabeus crater, a good correlation also exists with the maximum hydrogen concentration (according LEND measurements), minimum of average temperature (according Diviner data) and maximum floor depth (according LOLA data). This correlation is shown in Figure 5. It is a task for future work to understand why the PSRs in Shoemaker and Cabeus craters present strong

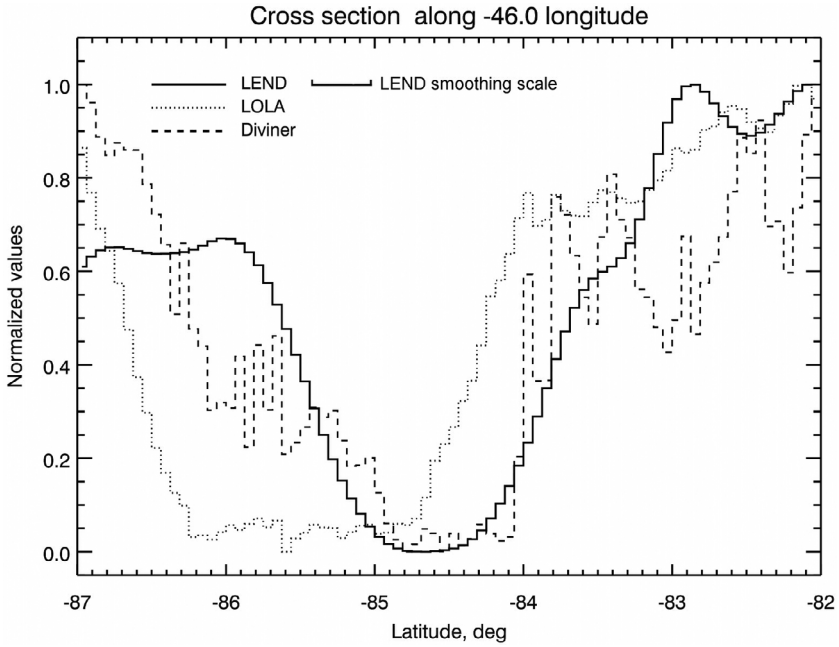

Figure 5. A cross-section in latitude at −46.0° longitude of the Cabeus crater for the LEND (solid line), LOLA (dotted line) and Diviner (dashed line) data. "LEND smoothing scale" corresponds to a FWHM of 10 km of the collimated detectors. The minimum of neutron flux (maximum of hydrogen) is well correlated with minimum of surface average temperature. Both minima are located at bottom part of the crater wall close to its floor.

enhancement of hydrogen concentration, but PSRs in Haworth and Faustini craters do not.

[32] Moreover, there are several PSRs with areas greater than 300 km^2 showing some epithermal neutron excess rather than suppression in comparison with local background. There are two possible reasons for epithermal neutron enhancements:

[33] 1. All found enhancements have statistical significance less than 3σ and, therefore, they may be a statistical fluctuations of measured signal;

[34] 2. All tested PSR are located inside the general poleward neutron suppression with deepest suppression ∼5%. This general suppression has been explained by general enhancement of H concentration in regolith with increasing of latitude. Therefore, some area above ±70° latitude may have higher epithermal neutron flux in comparison with surrounding regions at same latitude in case if this area is drier than its surrounding regions. In this case observed neutron enhancement must be less of equal to ∼5% taking into account the statistical uncertainty of found value.

[35] This leads us to the conclusion that large PSRs with sizes greater than the LEND FOV are not strong sources of neutron suppression of epithermal neutron flux as was previously thought. Data show that large PSRs do not appear to be local spots of epithermal neutron flux suppression. In some particular cases they show significant but moderate depression of epithermal neutron flux in comparison with nearby values of neutron flux attributed to average extended polar suppression in sunlit areas. Assuming a homogeneous model for the regolith, we may estimate a higher hydrogen abundance of several hundred ppm, which does not require the presence of traces of dirty water ice. However, the depth distribution inside such PSRs is more complicated.

4. Statistical Properties of Large PSRs

[36] In this section we continue the discussion of possible hydrogen enhancement in PSRs, focusing not on the most significant cases discussed in the previous section but applying statistical methods to the whole ensemble of PSRs.

[37] The total number of PSRs according to the latest LOLA illumination maps selected for this study is 344 for both lunar poles. There are 298 PSRs (summing north and south PSRs) having areas less than 100 km^2, which is less than LEND spatial resolution (group #1), 28 PSRs with area between 100 and 200 km^2, which are comparable with LEND spatial resolution (group #2), and 18 PSRs having an area larger than 200 km^2, which are easily resolved by LEND (group #3). The minimum size of PSRs included in this data set is limited by the shortest available observation time made by LEND and corresponds to spots of a few kilometers in diameter. The minimum LEND data acquisition time interval is 1 s. During this time LRO covers a distance of ∼1.6 km on the Moon's surface.

[38] In this section we study and compare statistical properties of PSRs distributed into these three different groups paying special attention to groups 2 and 3 with large PSR surface areas.

[39] In our first test we look at the distribution of the local suppression parameter (defined in expression 1) and its upper limit (defined in expression 2) as a function of exposure time (LEND observation time of a given PSR). Formally speaking, the local suppression parameter (following

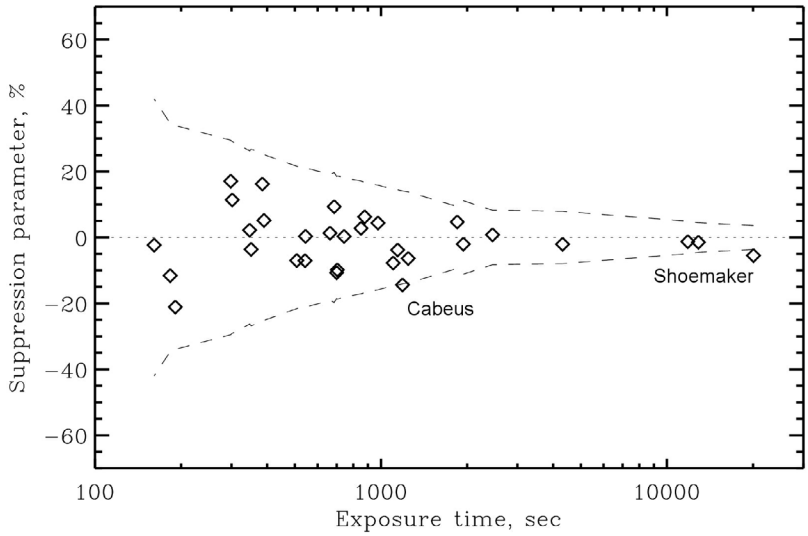

Figure 6. Local suppression/excess parameters (see expression (1)) measured for each large (area >100 km^2) southern PSR, presented as a function of exposure time accumulated during LEND observations for each PSR. The dashed lines correspond to the 3σ upper limits, Γ (see expression (2)), for excess (positive values) and suppression (negative values), respectively.

from expression 1) may take both negative and positive values. In the first case, it indicates that the counting rate of neutron flux measured inside the PSR is smaller than the average counting rate in the local sunlit vicinity. In the second case, it shows that local vicinity emits fewer neutrons than observed inside the PSR and local suppression parameter in reality turns into local excess parameter. In Figures 6 and 7 we present distributions of the measured local suppression/excess parameters as a function of exposure time for the selected south polar (Figure 6) and north polar (Figure 7) PSRs from groups 2 and 3 with areas >100 km^2. Local suppression parameter values, significant at the 3σ level and higher, are located outside the dashed lines and values of lower significance are inside the lines. In these figures one can see the largest PSRs (larger areas roughly correspond to longer exposure times) have high counting statistics and as a result small statistical errors. Only two cases of significant suppression are seen in the south (Shoemaker and Cabeus discussed in the previous section) and one case approaching the 3σ significance level in the north (Rozhdestvensky U crater). For these PSRs the local suppression parameter ranges from −5 to −15%. Many other large PSRs, some with even less statistical error, have local suppression parameter within the same range, but well

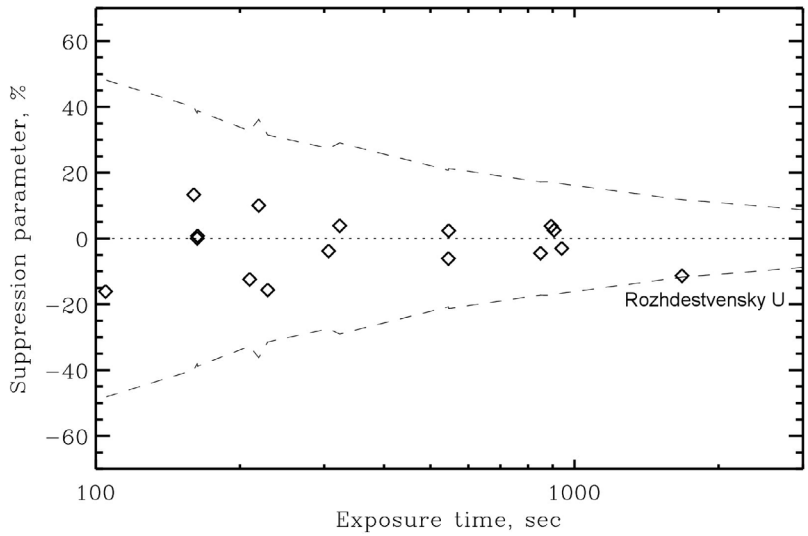

Figure 7. Local suppression/excess parameters (see expression (1)) measured for each large (area >100 km^2) northern PSR, presented as a function of exposure time accumulated during LEND observations for each PSR. The dashed lines correspond to the 3σ upper limits, Γ (see expression (2)), for excess (positive values) and suppression (negative values), respectively.

below the 3σ significance level. Moreover, there are several large PSRs (with surface area 300–400 km^2) displaying excess neutron flux instead of suppression. This leads to the conclusion that ordinary randomly selected PSRs with area greater than 300–400 km^2 do not necessarily manifest local neutron suppression larger than a few percent in comparison with local surrounding sunlit areas.

[40] In the previous section we have analyzed individual PSRs and were able to select only a few of them with significant local neutron suppression. On the other hand (see Table 1), there are many showing negative values of the local suppression parameter which could not be considered significant because their statistical uncertainty is too high. To decrease uncertainty one may combine PSRs in different groups and try to test the hypothesis that the distribution of counting rates within this given group is statistically different from the distribution of counting rates in the sunlit areas surrounding the PSRs included in the group. The counting rate in the sunlit areas is known very well (because of their large area and, as a result, enormous counting statistics) with the accuracy 10–100 times better than counting statistics for measurements inside the PSRs. The main point of the statistical analysis suggested in this section is to reduce local background counting rate to the same uncertainty level as observed in the PSRs and then to compare it with distribution of PSRs counting rates. The key value in such simulation is a PSR's exposure time. It defines the statistical uncertainty showing how many counts have been collected by LEND detectors during observation of the given PSR. Using counting rate B_i (counts per seconds) in the sunlit area and PSR exposure time T_i (seconds) one may simulate the counting rate S_i (counts per seconds) inside a PSR using Poisson statistic by the following formula:

$$S_i = C_i^{sim}/T_i, \tag{3}$$

Where C_i^{sim} is the randomly selected number of counts from the Poisson distribution with mean value $B_i \times T_i$.

[41] From expression (1) we may estimate a simulated local neutron suppression parameter as

$$P_i^{sim} = \frac{S_i - B_i}{1.7} \times 100\%. \tag{4}$$

Following this method it is possible to estimate the local neutron suppression parameter for each PSR from the local background counting rate which is weighted with the exposure time of the PSR (thereby weighted with the real statistical uncertainty attributed to the PSR) and randomized using Poisson statistics.

[42] The next step in our approach is to ensemble PSR groups for such analysis. We limited our selection to groups 1–3 already introduced in the beginning of the section. This selection criterion combines PSRs according to two important properties: 1) corresponding PSR surface area and LEND field of view, 2) combining PSRs with similar statistical uncertainties.

[43] For each group of PSRs we have created two distributions. The first represents the measured local neutron suppression parameter (presented in Table 1). The second one is a Monte Carlo simulation of the local neutron suppression parameter using equations (3) and (4). The comparison between these two distributions may indicate if we are able to explain the observed diversity of PSR suppressions (within given groups 1–3) just by statistical variations of counting rates measured at the nearby sunlit areas. To make this comparison robust we have used two well-known statistical criteria. First is the Student's t-test [e.g., *Press et al.*, 2007]. It tests the null hypothesis that the means of two normally distributed populations are equal. Here, we suppose that our two tested samples of real and simulated PSR suppressions belong to a normal distribution, but may have different mean values. Using sample parameters such as mean value and variance we may create a t-statistic parameter and check the probability that it follows a Student's t distribution. Another criterion is based on the Kolmogorov-Smirnov test or K-S test [e.g., see *Press et al.*, 2007]. It is a nonparametric test that can be used to compare two samples by quantifying the distance between the empirical distribution functions of two samples. It tests the null hypothesis (calculates the probability) that the samples are drawn from the same distribution.

[44] The real and simulated distributions of local neutron suppression parameter for the group #1 with 298 smallest PSRs are presented in Figure 8. Even from a visual comparison, it is clear that two distributions are very close to each other. This is confirmed by both test criteria. The K-S test shows that measured and simulated distributions for group #1 display the same statistics with the probability of 97%. Verification based on the Student's t-test shows that these distributions have the same mean value with a probability greater than 60%. So, we may conclude that statistical criteria cannot distinguish between neutron emissions inside PSRs with area <100 km^2 and in the sunlit areas around them.

[45] Group #2 includes 28 intermediate PSRs with surface areas between 100 km^2 and 200 km^2 with the average area of $\sim$132 km^2. These PSRs are comparable with the LEND footprint and could be resolved by LEND provided they differ from the local vicinity and have enough counting statistics to measure this difference. The comparison between samples of measured and simulated counting rates for this group (presented in Figure 9) shows that the probability of coincidence is lower than was found for group #1, but is still too large to conclude that these distributions are statistically different. The value of the t-statistic parameter estimated for these samples may be randomly selected from the Student's t-distribution with a probability of about 30%, which is enough to make the statement that these distributions could have the same mean values of local suppression. The K-S test shows that shapes of the two distributions can be fitted to each other with a probability of 20%, which is also too high to distinguish them with high significance. We may only summarize that medium-sized PSRs from group #2 tend to emit fewer neutrons then surrounding sunlit areas, but this difference is small in comparison with statistical uncertainty and may be explained by random process of counting statistic, but not a physical difference in the mechanism of neutron emission.

[46] Finally, group #3 includes the 18 largest PSRs with individual surface area greater than 200 km^2 and with average area $\sim$407 km^2, which is significantly larger than the area of LEND footprint. The comparison between observed and simulated distributions of counting rates for group #3 is presented in Figure 10. It is seen that their shapes

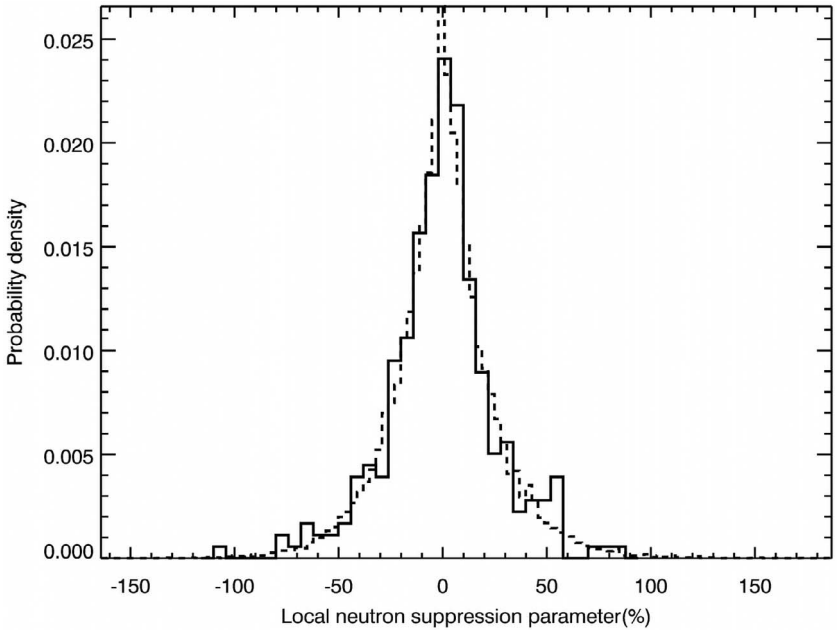

Figure 8. Distribution of counting rates measured inside small PSRs (surface area <100 km^2) shown in solid black. The distribution of simulated counting rates for these PSRs is shown by the dashed line.

and mean values are quite different. If one uses the K-S test to check if these samples are taken from the same distribution the most probable answer will be "no." The probability to coincide is only about 1% and that is very close to the 3σ level (probability = 0.27%) commonly used to define an unlikely event. The Student's t-test also shows that the probability that these samples belong to a normal distribution with same mean value is fairly low, ~0.7%. Analyzing these results we may state that the neutron flux measured in large area PSRs is probably less than the neutron flux in nearby sunlit areas. In our statistical analysis we also estimate the average local suppression, which would be necessary to achieve consistency between measured and simulated distributions. We shift the simulated distribution of the local neutron suppression parameter for the large PSRs until both statistical criteria show maximal probability of coincidence

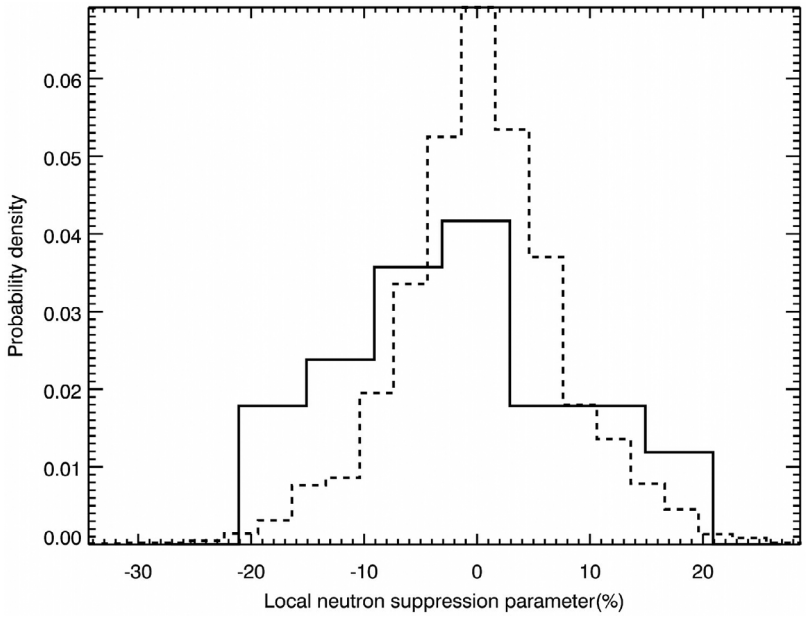

Figure 9. Distribution of counting rates measured inside medium-sized PSRs (with surface areas 100–200 km^2) shown by solid black line. The distribution of simulated counting rates for these PSRs based on hypothesis about zero local suppression is shown by the dashed line.

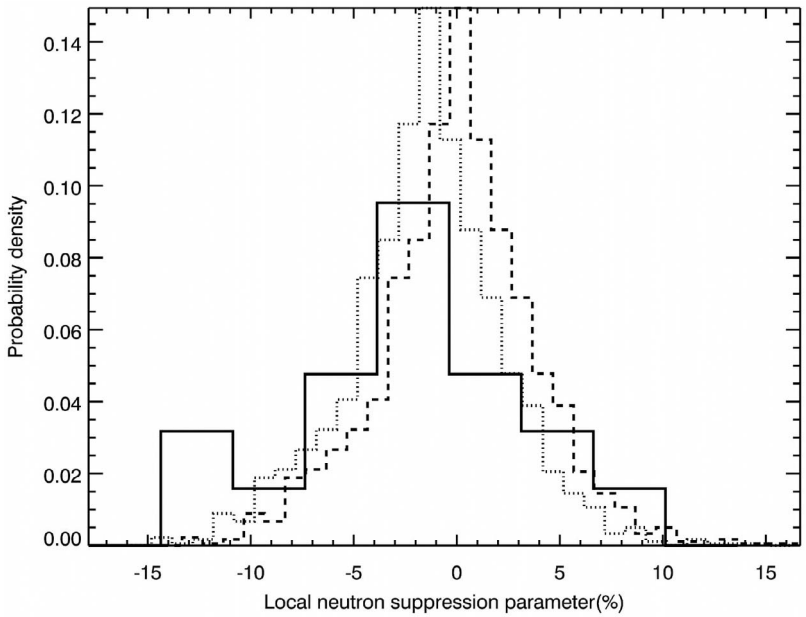

Figure 10. Distribution of counting rates measured inside large PSRs (surface area >200 km^2) shown by solid black line. The distribution of simulated counting rates for these PSRs based on assumption of zero local suppression is shown by the dashed line. The distribution of simulated counting rates for these PSRs based on assumption of best fit local suppression is shown by the dotted line.

between the shifted distribution and the distribution of real measured suppression. The best shift value corresponds to a local suppression of $-2.2 \pm 1.5\%$. The result of this analysis is shown in Figure 10. Summarizing, one may say that large area PSRs belonging to group #3 display local suppression and may be treated as spots with enhanced hydrogen content, but the value of the average local suppression is too small to make definite statement that large PSRs are very well localized and isolated spots with very high hydrogen content which may interpreted as water ice.

5. Conclusions

[47] Both analyses of individual PSRs and studies of groups of PSRs have shown that these spots of extreme cold at the lunar poles are not associated with a strong effect of suppression of epithermal neutron emission. To estimate the local effect of suppression in PSRs, we have compared the count rates to the sunlit vicinity around them. We found only three large PSRs, Shoemaker and Cabeus in the south and Rozhdestvensky U in the north, which manifest significant neutron suppression, about -5.5% to -14.9%. All other PSRs have much smaller suppression, no more than few percent, if at all. Some PSRs even display a positive deviation, implying an excess of neutron emission in respect to the sunlit vicinity around them.

[48] Testing PSRs collectively, we have not found any statistically significant average suppression. Only the group of 18 large PSRs, with area >200 km^2, shows a marginal effect of small average suppression of about 2%, with small statistical confidence. LEND will collect more data and provide better counting statistics for PSRs, but even now the data is enough for definite conclusion that PSRs at both poles are not reservoirs of large deposits of water ice, which would be seen as depressions in the emission map of lunar neutrons. The major effect of extended suppression of neutrons at the lunar poles is associated with sunlit surfaces, and one has to test the local neutron suppression regions (NSRs) outside the permanent darkness of PSRs.

[49] On the other hand, the exceptional cases of Shoemaker, Cabeus and Rozhdestvensky U show that large enhancements of hydrogen exist in some particular PSRs. Comparison of data for neutrons, surface altimetry and surface temperature shows very good agreement between the shadow in Shoemaker and emission of epithermal neutrons (see Figure 4). The presence of water ice has also been experimentally confirmed for regolith in Cabeus ($5.6 \pm 2.9\%$) by direct measurements of the plume from the LCROSS impact.

[50] The physical processes for the trapping of volatiles is not as straightforward as previously thought, with the trapping of water molecules from the exosphere in cold spots of permanent shadow. One must study more complex physical models, where all PSRs are not the principal depository of lunar water and where there should be some physical difference between PSRs, which make some better candidates for higher water content compared with the regolith in nearby sunlit regions.

[51] **Acknowledgments.** We wish to thank the International Space Science Institute (ISSI, Bern, Switzerland) for the support of research (included in the framework of international team "Nuclear Planetology" in 2007–2010) presented in this paper.

References

Arnold, J. R. (1979), Ice in the lunar polar regions, *J. Geophys. Res.*, *84*, 5659–5668.

Clark, R. N. (2009), Detection of adsorbed water and hydroxyl on the Moon, *Science*, *326*(5952), 562–564, doi:10.1126/science.1178105.

Colaprete, A., et al. (2010), Detection of water in the LCROSS ejecta plume, *Science*, *330*(6003), 463–468, doi:10.1126/science.1186986.

Crider, D., and R. Vondrak (2000), The solar wind as a possible source of lunar polar hydrogen deposits, *J. Geophys. Res.*, *105*(E11), 26,773–26,782, doi:10.1029/2000JE001277.

Crider, D., and R. Vondrak (2003), Space weathering effects on lunar cold trap deposits, *J. Geophys. Res.*, *108*(E7), 5079, doi:10.1029/2002JE002030.

Eke, V. R., L. F. A. Teodoro, and R. C. Elphic (2009), The spatial distribution of polar hydrogen deposits on the Moon, *Icarus*, *200*(1), 12–18, doi:10.1016/j.icarus.2008.10.013.

Elphic, R. C., D. J. Lawrence, W. C. Feldman, B. L. Barraclough, S. Maurice, A. B. Binder, and P. G. Lucey (1998), Lunar Fe and Ti abundances: Comparison of Lunar Prospector and Clementine data, *Science*, *281*, 1493–1496, doi:10.1126/science.281.5382.1493.

Elphic, R. C., V. R. Eke, L. F. A. Teodoro, D. J. Lawrence, and D. B. J. Bussey (2007), Models of the distribution and abundance of hydrogen at the lunar south pole, *Geophys. Res. Lett.*, *34*, L13204, doi:10.1029/2007GL029954.

Fa, W., M. A. Wieczorek, and E. Heggy (2011), Modeling polarimetric radar scattering from the lunar surface: Study on the effect of physical properties of the regolith layer, *J. Geophys. Res.*, *116*, E03005, doi:10.1029/2010JE003649.

Feldman, W. C., B. L. Barraclough, S. Maurice, R. C. Elphic, D. J. Lawrence, D. R. Thomsen, and A. B. Binder (1998a), Major compositional units of the Moon: Lunar Prospector thermal and fast neutrons, *Science*, *281*, 1489–1493, doi:10.1126/science.281.5382.1489.

Feldman, W. C., S. Maurice, A. B. Binder, B. L. Barraclough, R. C. Elphic, and D. J. Lawrence (1998b), Fluxes of fast and epithermal neutrons from Lunar Prospector: Evidence for water ice at the lunar poles, *Science*, *281*, 1496–1500, doi:10.1126/science.281.5382.1496.

Feldman, W. C., et al. (2001), Evidence for water ice near the lunar poles, *J. Geophys. Res.*, *106*(E10), 23,231–23,251, doi:10.1029/2000JE001444.

Feldman, W. C., et al. (2004), Gamma-Ray, Neutron, and Alpha-Particle Spectrometers for the Lunar Prospector mission, *J. Geophys. Res.*, *109*, E07S06, doi:10.1029/2003JE002207.

Gasnault, O., W. C. Feldman, S. Maurice, I. Genetay, C. d'Uston, T. H. Prettyman, and K. R. Moore (2001), Composition from fast neutrons: Application to the Moon, *Geophys. Res. Lett.*, *28*(19), 3797–3800, doi:10.1029/2001GL013072.

Lawrence, D. J., W. C. Feldman, R. C. Elphic, J. J. Hagerty, S. Maurice, G. W. McKinney, and T. H. Prettyman (2006), Improved modeling of Lunar Prospector neutron spectrometer data: Implications for hydrogen deposits at the lunar poles, *J. Geophys. Res.*, *111*, E08001, doi:10.1029/2005JE002637.

Litvak, M. L., et al. (2012), Global maps of lunar neutron fluxes from the LEND instrument, *J. Geophys. Res.*, doi:10.1029/2011JE003949, in press.

Maurice, S., D. J. Lawrence, W. C. Feldman, R. C. Elphic, and O. Gasnault (2004), Reduction of neutron data from Lunar Prospector, *J. Geophys. Res.*, *109*, E07S04, doi:10.1029/2003JE002208.

Mazarico, E., G. A. Neumann, D. E. Smith, M. T. Zuber, and M. H. Torrence (2011), Illumination conditions of the lunar polar regions using LOLA topography, *Icarus*, *211*(2), 1066–1081, doi:10.1016/j.icarus.2010.10.030.

McClanahan, T. P., et al. (2012), Correlated observations of epithermal neutrons and polar illumination models from orbital neutron detectors, Abstract 234 presented at the 43rd Lunar and Planetary Science Conference, Lunar and Planet. Inst., The Woodlands, Tex., 19–23 March.

Mitrofanov, I. G., et al. (2008), Experiment LEND of the NASA Lunar Reconnaissance Orbiter for high-resolution mapping of neutron emission of the Moon, *Astrobiology*, *8*(4), 793–804, doi:10.1089/ast.2007.0158.

Mitrofanov, I. G., et al. (2010a), Lunar Exploration Neutron Detector for the NASA Lunar Reconnaissance Orbiter, *Space Sci. Rev.*, *150*(1–4), 183–207, doi:10.1007/s11214-009-9608-4.

Mitrofanov, I. G., et al. (2010b), Hydrogen Mapping of the Lunar South Pole Using the LRO Neutron Detector Experiment LEND, *Science*, *330*(6003), 483–486, doi:10.1126/science.1185696.

Nozette, S., C. L. Lichtenberg, P. Spudis, R. Bonner, W. Ort, E. Malaret, M. Robinson, and E. M. Shoemaker (1996), The Clementine Bistatic Radar Experiment, *Science*, *274*(5292), 1495–1498, doi:10.1126/science.274.5292.1495.

Nozette, S., P. Spudis, M. Robinson, D. B. J. Bussey, C. Lichtenberg, and R. Bonner (2001), Integration of lunar polar remote-sensing data sets: Evidence for ice at the lunar south pole, *J. Geophys. Res.*, *106*(E10), 23,253–23,266, doi:10.1029/2000JE001417.

Pieters, C. M., et al. (2009), Character and spatial distribution of OH/H_2O on the surface of the Moon seen by M3 on Chandrayaan-1, *Science*, *326*(5952), 568–572.

Press, W., S. Teukolsky, W. Vetterling, and B. Flannery (2007) *Numerical Recipes*, Cambridge Univ. Press, Cambridge, U. K.

Simpson, R. A., and G. L. Tyler (1999), Reanalysis of Clementine bistatic radar data from the lunar south pole, *J. Geophys. Res.*, *104*(E2), 3845–3862, doi:10.1029/1998JE900038.

Smith, D. E., et al. (2010), The Lunar Orbiter Laser Altimeter Investigation on the Lunar Reconnaissance Orbiter Mission, *Space Sci. Rev.*, *150*(1–4), 209–241, doi:10.1007/s11214-009-9512-y.

Spudis, P. D., et al. (2010), Initial results for the north pole of the Moon from Mini-SAR, Chandrayaan-1 mission, *Geophys. Res. Lett.*, *37*, L06204, doi:10.1029/2009GL042259.

Sunshine, J. M., T. L. Farnham, L. M. Feaga, O. Groussin, F. Merlin, R. E. Milliken, and M. F. A'Hearn (2009), Temporal and spatial variability of lunar hydration as observed by the Deep Impact spacecraft, *Science*, *326*(5952), 565–568.

Watson, K., B. C. Murray, and H. Brown (1961), The behavior of volatiles on the lunar surface, *J. Geophys. Res.*, *66*(9), 3033–3045, doi:10.1029/JZ066i009p03033.